ICAS PAPER No. 72 – 21

SOME RESULTS OF INVESTIGATIONS OF PROBLEMS
RELATING TO SUPERSONIC AND HYPERSONIC COMBUSTION

by
E. Krause, F. Maurer and H. Pfeiffer
DFVLR, Porz-Wahn, Germany

The Eighth Congress of the International Council of the Aeronautical Sciences

INTERNATIONAAL CONGRESCENTRUM RAI-AMSTERDAM, THE NETHERLANDS
AUGUST 28 TO SEPTEMBER 2, 1972

Price: 3. Dfl.

SOME RESULTS OF INVESTIGATIONS OF PROBLEMS RELATING TO SUPERSONIC AND HYPERSONIC COMBUSTION

E. Krause[+], F. Maurer, and H. Pfeiffer

DFVLR-Institut für Angewandte Gasdynamik
Porz-Wahn, Germany

Abstract

Experimental and theoretical investigations of supersonic and hypersonic combustion processes are presently being carried out at the "DFVLR-Institut für Angewandte Gasdynamik". At supersonic Mach numbers external combustion is employed to generate aerodynamic side forces on a flat plate. Secondary air is injected normal to the main stream through a slot in the wall. Stable combustion in the recirculation region upstream of the slot is achieved by injecting hydrogen normal to the wall and initiating the combustion through a spark plug. The flame stabilizes after the initiation and the heat released in the recirculation region causes the separation point to move upstream. Surveys of the wall pressure show that a large region of high pressure can be generated. The resulting side forces are large compared with those generated through aerodynamic spoiler action without heat release.

At hypersonic Mach numbers the mixing process during the induction period is studied by injecting a foreign gas tangentially to the plate. The experimental results obtained so far indicate that transition to turbulent flow did not occur at free stream Mach numbers of about 10 and Reynolds numbers per meter of about $4 \cdot 10^6$. In the mixing zone detailed measurements of static and stagnation pressures, total temperatures and concentration of the injected gas enable a clear picture of the flow behaviour. Above all a rapid concentration decay was noted immediately downstream from the slot. This happened despite of the fact that the flow remained laminar. The experimental data obtained at hypersonic Mach numbers agree with results obtained by numerical integration of the boundary-layer equations for laminar flows. To ensure the validity of these equations the static pressure of the injected gas was adjusted to the local static pressure on the plate which remained approximately constant throughout the mixing region. For comparison-calculations the initial- and boundary conditions of the experiments were used in the numerical solution. Complete flow field analysis can be obtained with this solution for chemically frozen flows and flows in chemical equilibrium approximated by a flame sheet. Multicomponent diffusion is taken into account for laminar flows while for turbulent flows results have been obtained by using an eddy-viscosity model for the turbulent viscosity and by defining the thermal conductivity and diffusion coefficients through turbulent Prandtl- and Schmidt numbers.

Introduction and Statement of the Problem

As hypersonic flight vehicles and even supersonic vehicles necessitate integrated propulsion systems the interaction between the external flow field about the vehicle and the flow region where the heat is released became a major field of interest. Presently, various modes of supersonic combustion are under investigation [1]. In the "DFVLR-Institut für Angewandte Gasdynamik" a research programme was set up several years ago to study two specific problems of the combustion process for various flight conditions: The first problem to be investigated is that of a supersonic flow passing over a flat plate and interacting with a gaseous combustible medium being injected normal to the main stream. As normal injection followed by heat release of the exothermic reaction between the oxygen of the external flow and the gaseous fuel cannot be considered realistically in the frame of boundary-layer theory, it was decided to study this problem for hard-blowing conditions: By separating the boundary layer through secondary air injected normally through a slot two recirculation regions are generated, one upstream and one downstream from the injection slot. In the early part of the investigation it was soon discovered that continuous and stable combustion was possible in the upstream recirculation region if gaseous fuel (in this case hydrogen) was added to the separated flow through a slot (or holes). Theoretical analysis of the problem is difficult because of the flow reversal in the injection region,

[+] Now: Aerodynamisches Institut,
Technische Hochschule Aachen

shock interaction and other phenomena as possible transitional flow with a complicated reaction taking place in the recirculation region. Nevertheless, a one-dimensional analysis was carried out by the second author. The major results of that investigation are published in Ref. [2] and will not be repeated here. Surveys of the wall pressure show the effect of heat release, and the major results of the experimental investigation will be given in this paper. Of the important parameters of the problem, the free stream Mach number and the mass flux of both, injected secondary air and hydrogen were varied in the experiments in order to determine their influence on the pressure distribution and the extent of the separated region.

The second problem under investigation is an experimental and theoretical flow field analysis of tangential slot injection of a foreign gas at hypersonic free stream conditions. When the static pressure in the slot is assumed to be equal to that of the external flow boundary-layer theory can be applied. Numerical solutions developed for this problem enable one to analyse the initial-boundary-value problem for complicated initial condititons. The solution, only briefly described in this paper is capable of taking into account diffusion effects of three non-reacting chemical components when the mixing process is laminar. This is also possible when a simple chemical model for equilibrium conditions, as described by the flame sheet approximation, is assumed. The solution has been applied to turbulent mixing flows with initial- and boundary conditions as described before. For closure of the problem eddy-viscosity-type models are chosen for the turbulent viscosity, thermal conductivity and diffusion coefficient.

For laminar flows, the solution is being used to determine the influence of the dominant parameters of the problem, in particular on concentration decay, heat transfer or wall temperature distribution and shearing stress at the wall. Simultaneous experimental investigations of static and stagnation pressures, total temperature and concentration profiles serve to substantiate the theoretical findings. The primary difficulties of the experimental investigation consist in the concentration measurement at high Mach numbers. As the static pressures on the plate are of the order of one Torr considerable time is necessary to extract enough flow material in a probe for an accurate concentration measurement. This difficulty can, however, be circumnavigated as the small hypersonic facility H1 of the "DFVLR-Institut für Angewandte Gasdynamik" enables running times of the order of twenty minutes to half an hour, and first concentration measurements have been obtained for helium-air mixtures. The investigation of normal injection and burning of hydrogen at supersonic speeds will be described first. Thereafter results will be presented for the investigation of tangential slot injection at hypersonic speeds with and without combustion. Finally a brief account of the numerical solution along with some results obtained through numerical integration of the boundary-layer equations will be given.

Normal Injection and Combustion of Hydrogen at Supersonic Speeds.

Wind Tunnel and Description of Experimental Conditions.

The experiments described in this section were carried out in the vertical free-jet tunnel (23 cm in diameter) of the 30 by 30 cm blow-down facility of the DFVLR in Porz-Wahn. Results were obtained for the free stream Mach numbers M_∞ = 2.25, 2.80, and 3.20. The static pressure in the free stream was about 1 atm for the first two Mach numbers and about 0.68 atm for M_∞ = 3.2. All tests were conducted at a stagnation temperature T_o of 290 K. The tunnel was always started first and then the secondary air was injected into the main stream at various pressure ratios, ranging from 1 to 60. The particular pressure ratio chosen was kept constant for the test while hydrogen was injected at various mass flux rates. Ignition was initiated for the largest injected mass flux with a spark plug. After the flame had stabilized the plug was retracted pneumatically out of the test section. For each mass flux rate of the hydrogen pressure measurements were obtained along the center line of the model with a scanivalve. Data were recorded upstream and downstream from the injection slot for the secondary air, which had a width of 0.35 mm. The hydrogen was injected through holes, being 0.3 mm in diameter. They were arranged 30 mm upstream from the slot for

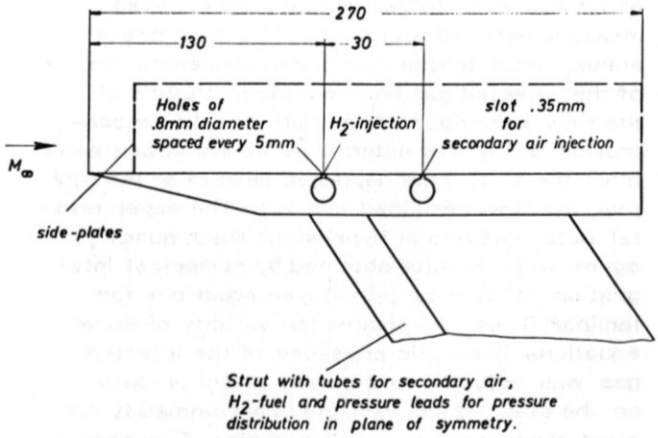

FIG. 1. Schematic of Test Model for Normal Injection and Burning of Hydrogen.

the secondary air in a row, being 5 mm apart from each other. The model is depicted schematically in Fig. 1, and the actual model is shown in Fig. 2 as mounted in the test section.

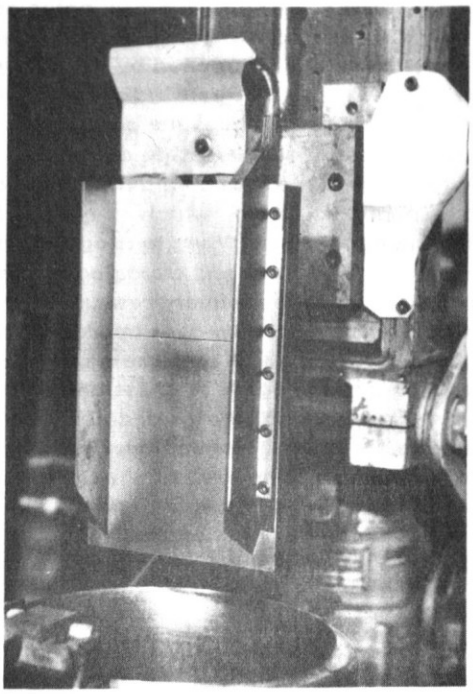

FIG. 2. Test Model for Normal Injection and Burning of Hydrogen as Mounted in the Tunnel.

In order to detect three-dimensional effects side plates (shown in Fig. 2) were fastened on both sides of the model and tests were run with and without them. Although three-dimensional effects present in the flow could not completely be eliminated by the side-plates the experimental results give an indication of the cross flow caused by the overpressure in the separated region. In Fig. 2 the arrangement of the holes for measuring the static pressure along the center line of the model is also visible.

Description of Experimental Investigation.

After the stabilisation of the flame could be achieved for all Mach numbers of interest the experimental investigation was divided into the following phases:

1. The wall pressure distribution was to be determined for each one of the free stream Mach numbers for constant mass flux of the secondary air but variable mass flux of the hydrogen.
2. The influence of the stagnation pressure of the secondary air on the wall pressure distribution and on the extent of the separated region was to be determined. Varying the stagnation pressure is equivalent to varying the mass flux of the secondary air. As the width of the slot was held constant only the influence of the stagnation pressure could be taken into account in the experimental results.
3. The influence of the free stream Mach number on the wall-pressure distribution and on the extent of the separated region upstream from the injection slot should be determined by comparing various measurements with other parameters held approximately constant.
4. The three-dimensionality of the flow should be detected by comparing experimental results obtained with and without side plates.

The details of this investigation are given in Refs. [2] and [3]. Here only the major results will be discussed by describing some of the pressure distributions determined experimentally. This is contained in the next section.

Discussion of Experimental Results.

The results presented in this section are taken from several series of tests conducted in the course of the investigation. To give an indication of the flow behaviour the overall flow pattern is shown in the schlieren pictures of Figs. 3 and 4 for tests without side plates at a free stream Mach number $M_\infty = 2.8$. It can be seen that the jet of the secondary air is not - as could be expected -

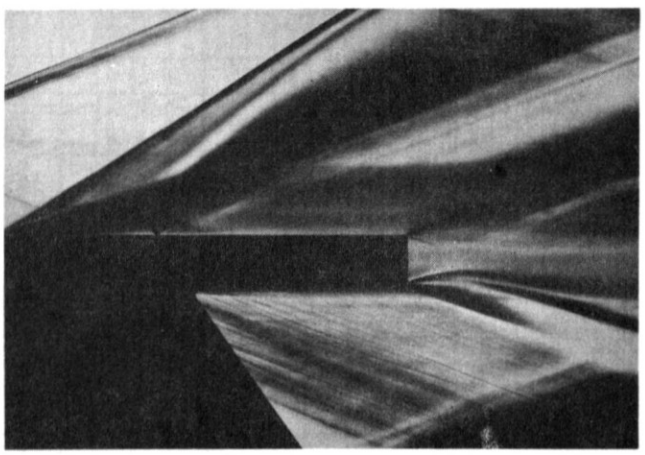

FIG. 3. Normal Injection and Burning of Hydrogen. (Shutter Speed 1/300 Sec. Continuous Light Source)

disintegrated through mixing with the hydrogen. Instead, it is rapidly deflected in the direction of the main stream and retains its jetlike nature a certain distance downstream from the slot. The secondary air therefore serves mainly to generate a separated region upstream from the slot where most of the hydrogen injected through the holes is oxydized by the oxygen of the main stream. It is also noted that the jet deflects the hot combustion products so that they cannot come close to the wall. The hot recirculation region is thus abruptly terminated and the air injected through the slot prevents the downstream portion of the plate to be

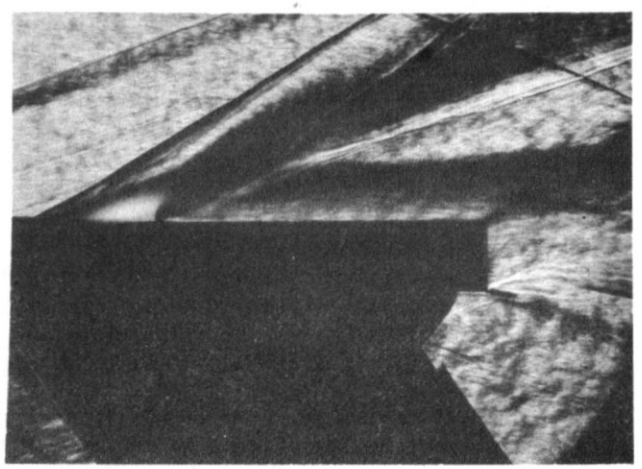

FIG. 4. Normal Injection and Burning of Hydrogen. Flame Made Visible by a Spark Flash.

heated up. In Fig. 4 the flame itself is made visible by a spark flash. The entire separated region upstream from the slot shows the glow of the flame which is not visible in Fig. 3 where a shutter speed of 1/300 sec was used,

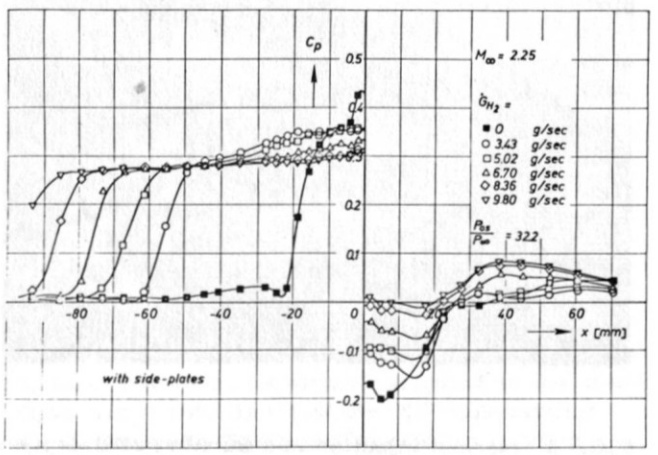

FIG. 5. Wall Pressure Distribution. Normal Injection and Burning of Hydrogen.

A typical pressure distribution is given for $M_\infty = 2.25$ in Fig. 5. The pressure ratio of the secondary air is $P_{OS}/P_\infty = 32.2$ and wall pressures are given for six different mass flux rates of hydrogen. The flow field without hydrogen injection and combustion is characterized by the curve for the wall pressure distribution indicated by the full squares. The maximum pressure coefficient upstream from the slot (the location of the slot coincides with the origin of the coordinate system) decreases rapidly to zero, which is typical for hard blowing conditions. When hydrogen is added to the flow at x = -30 mm and oxydized in the separated region the maximum overpressure is reduced to a value of 0.3 for the largest hydrogen mass flux injected. At the same time the separation point of the recirculation region is drastically moved upstream. The extent of the recirculation region is now three to five times larger than that generated without combustion. The pressure remains almost constant in the separated region and does not seem to depend strongly on the injected mass flux of the hydrogen. This seems to be more pronounced in the separated region downstream from the slot.

The influence of the freestream Mach number is indicated in Fig. 6. While the pressure ratio of

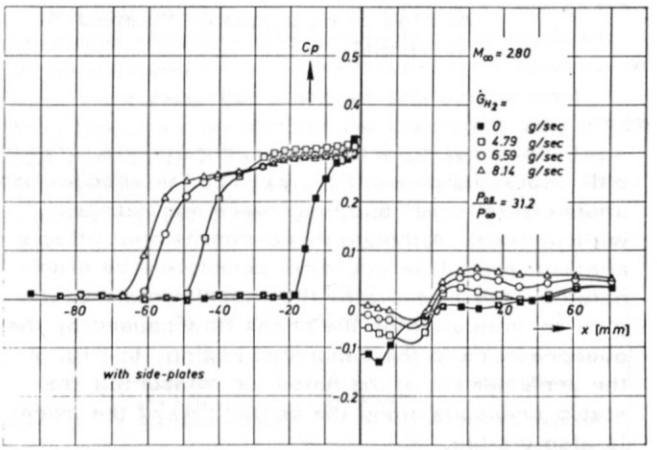

FIG. 6. Wall Pressure Distribution. Normal Injection and Burning of Hydrogen.

the secondary air is almost the same as before M_∞ is increased to 2.8. It can be seen that the maximum pressure with and without combustion is equal to 0.3 and is even less dependent on the amount of hydrogen injected. At the same time the separated region is smaller for the same amount of hydrogen injected. The Mach-number effect is even more pronounced for (Fig. 7) $M_\infty = 3.2$, for which

a larger mass flux of the secondary air was chosen. It is seen that

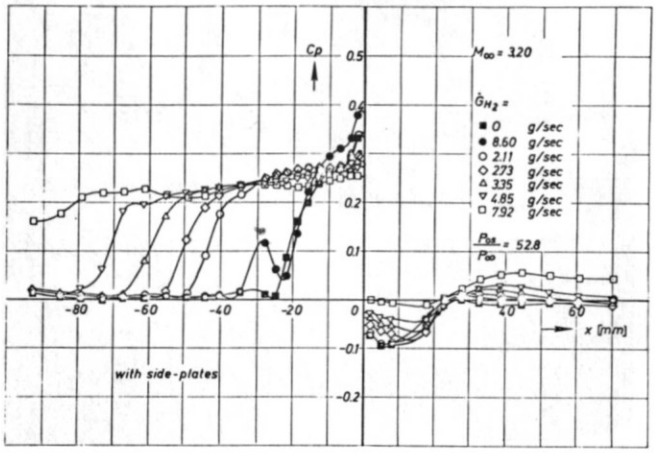

FIG. 7. Wall Pressure Distribution. Normal Injection and Burning of Hydrogen.

the maximum pressure drops to about 0.25 and does not reach the value given in the last figure although the pressure ratio of the secondary air was increased to 52.8.

The influence of the pressure ratio of the secondary air can be seen by comparing Fig. 6 with Fig. 8, where P_{os}/P_∞ is approximately half of the value given in Fig. 6. The maximum

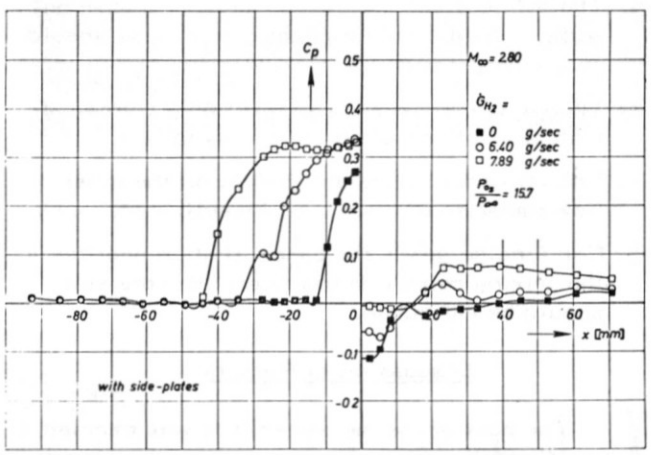

FIG. 8. Normal Injection and Burning of Hydrogen. Influence Stagnation Pressure of Injected Secondary Air. (See also FIG. 6.)

pressures remain almost the same while the length of the separated region is reduced by some 30 percent. The boundary layer in front of the separated region had undergone transition to turbulent flow in all cases described so far.

It is clear from the pressure distribution that cross flows must result from the overpressure to both sides of the model. Although the pressure curves shown in Figs. 5-8 were obtained with the side plates mounted on the model it cannot be concluded that the flow is strictly two-dimensional.

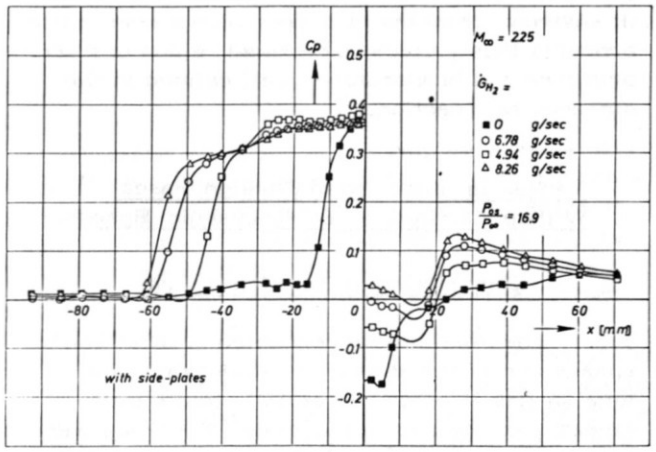

FIG. 9. Normal Injection and Burning of Hydrogen. Influence of Cross-Flows. (See FIG. 10.)

The influence of the side plates is shown for $M_\infty = 2.25$ in Figs. 9 and 10. When the side plates are removed the maximum static pressure remains unchanged while the separation point is noticeably moved downstream.

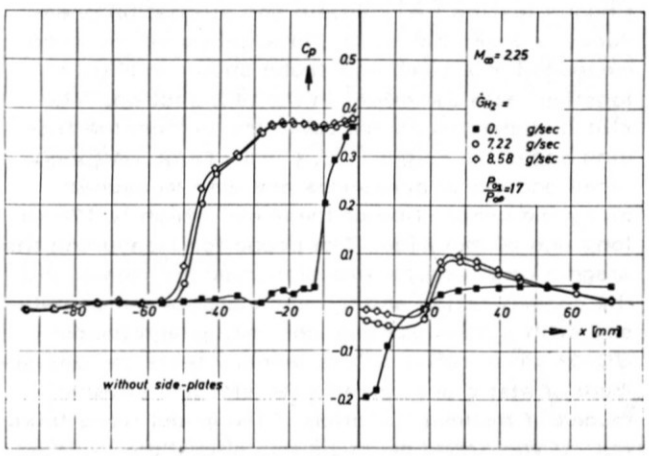

FIG. 10. Normal Injection and Burning of Hydrogen. Influence of Cross-Flows.

In summarizing the results reported in this section one can conclude that supersonic combustion may be used effectively to generate side forces much larger than those obtained without combustion. By injecting and burning of hydrogen in a separated region, enforced by a secondary stream of air injected normal to the main stream, the separation point can be moved upstream considerably and a high static pressure is observed in the entire separation region. At the same time the secondary air serves to protect the plate downstream from the slot from the hot combustion products thus yielding a confined region of high pressure and temperature, well defined in the streamwise direction.

Tangential Injection of Foreign Gases Without Combustion at Hypersonic Speeds.

Description of Test Conditions

The experiments conducted at hypersonic speeds are aimed at studying the mixing of a foreign gas injected tangentially to the main stream passing over a flat plate. The tests were carried out in the small hypersonic tunnel H 1 of the DFVLR in Porz-Wahn which allows tests at freestream Mach numbers M_∞ = 8.5, 10 and 15 with maximum Reynolds numbers per meter ranging from 10^7 at M_∞ = 8.5 to about 10^6 at M_∞ = 15.0. Extremely long test duration is made possible since the tunnel is connected to a large vacuum sphere of 2.10^3 m^3. As conical nozzles with an exit diameter of 16 cm are used, the main flow diverges slightly in the test section with a Mach number gradient along the center line of about 0.05 cm^{-1}. The electric heater allows a maximum possible stagnation temperature of 1400 K for continuous testing [4]. Static and stagnation pressures, concentration and total temperature were measured in a combined probe shown in Fig. 11 together with the model in the test section. The slot is arranged 35 mm downstream from the leading edge. Its height is 2.5 mm. Total temperatures and static pressures are also measured along the center line of the model which is 170 mm long and 60 mm wide. The probe for measuring the stagnation pressure was also used for measuring the concentration and the gas samples were analysed with a Beckman gas-chromatograph (model GC-2). In a series of preliminary tests the adjustment of static pressure in the slot and several modes of thermal isolation of the model were tried out. It was found necessary to shield the injected gas through a water cooling system in order to maintain a low temperature in the slot. After a calibration chart was constructed for the concentration measurements the following test programme was set up:

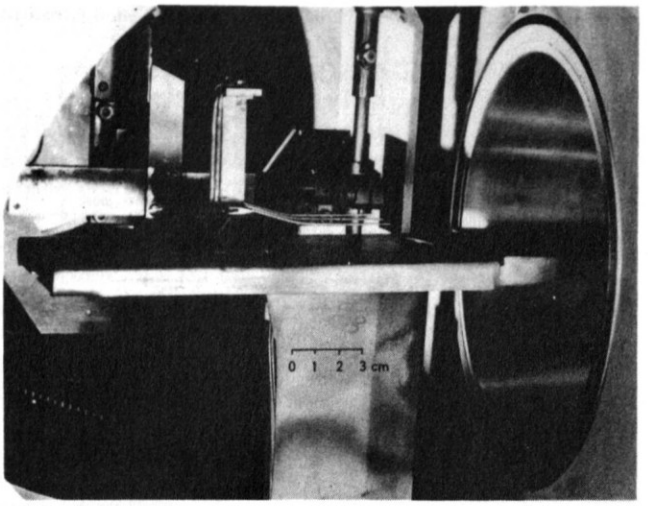

FIG. 11. Test Model for Tangential Slot Injection. Shown in Tunnel with Combined Probe.

Test Programme for Mixing Problems at Hypersonic Conditions.

1. The static and stagnation pressures, the total temperature, velocity and static temperature profiles were to be determined by using cold air for the injected gas.
2. The influence of the external Mach number on both, velocity and temperature profiles should be investigated.
3. The experimental results should be compared with predictions of numerical solutions.
4. The influence of the slot height on the other flow parameters should be investigated.
5. For foreign gases the concentration profiles in the mixing region downstream from the slot should be measured.

Discussion of Results

The bulk of the measurements was carried out by E. Will and detailed results of the phases 1 to 3 are reported in [5]. The schlieren pictures in Figs. 12 and 13 show two different flow configurations. For the flow shown in Fig. 12 the static pressure in the slot is higher than that of the surrounding flow and a shock wave is generated as a result of the expansion of the injected air. This case has not been considered in the experiments so far. As it was the aim to compute velocity, temperature and concentration profiles through boundary-layer theory only flow fields with ad-

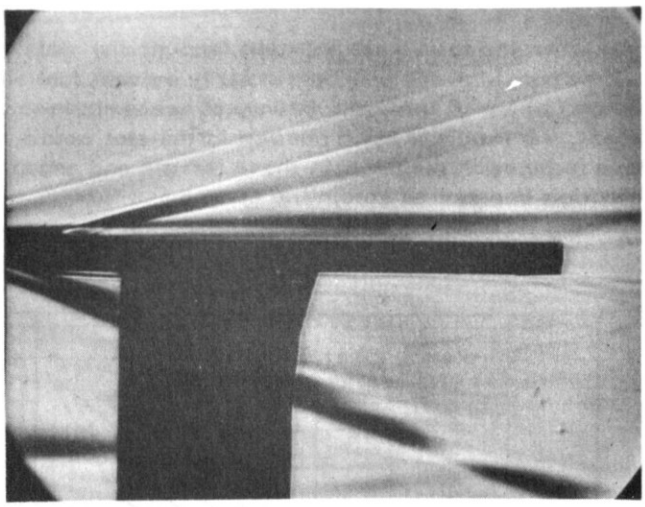

FIG. 12. Tangential Slot Injection. Static Pressure in the Slot Higher than in the Free-Stream.

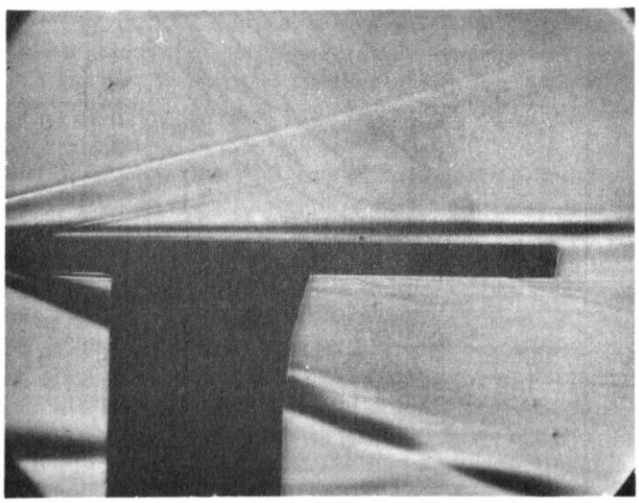

FIG. 13. Tangential Slot Injection. Static Pressure in the Slot Equal to that of the Free-Stream.

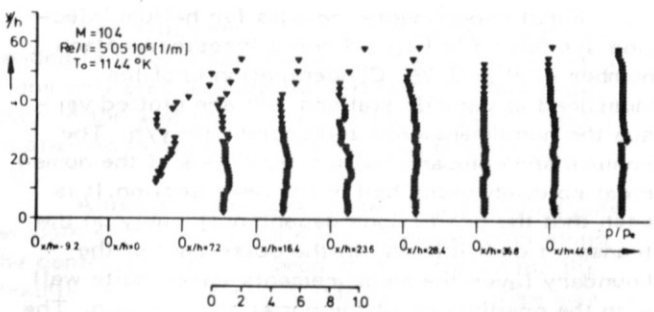

FIG. 14. Tangential Slot Injection. Measured Static Pressure Distribution.

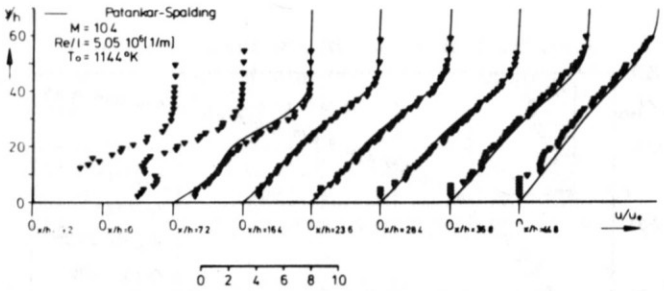

FIG. 15. Comparison of Experimentally and Numerically Determined Velocity Profiles.

justed static pressure in the slot were investigated. Such a flow is shown in Fig. 13. In comparison to Fig. 12 no shock is observed downstream from the slot. This was achieved by lowering the static pressure of the injected air until the shock disappeared. Static pressure profiles measured at a freestream Mach number of about 10.4 are depicted in Fig. 14. Plotted are the profiles of the static pressure for various x-stations (x = 0 designates the location of the slot). Disturbances of the order of 20 percent can be noted immediately upstream and downstream from the slot in the outer portion of the boundary layer. The disturbance is caused by the leading edge of the plate which gives rise to a weak shock also visible in the schlieren pictures Figs. 12 and 13. For the region of interest the pressure varies only little in the direction normal to the wall, so that the flow obeys the conditions imposed by boundary-layer theory. The profiles shown here are also representative for the other freestream Mach numbers investigated.

Examples for the third point of the programme are shown in Figs. 15 and 16. In Fig. 15 the velocity profiles as obtained in the experiments were compared with the predictions of Ref. [6] obtained by the numerical solution of [7]. The laminar nature of the flow in the mixing region is

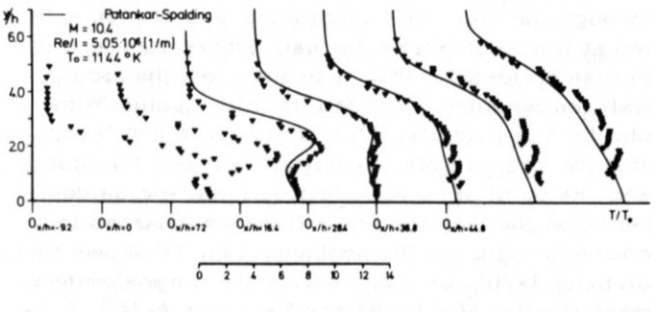

FIG. 16. Comparison of Experimentally and Numerically Determined Static Temperature Profiles.

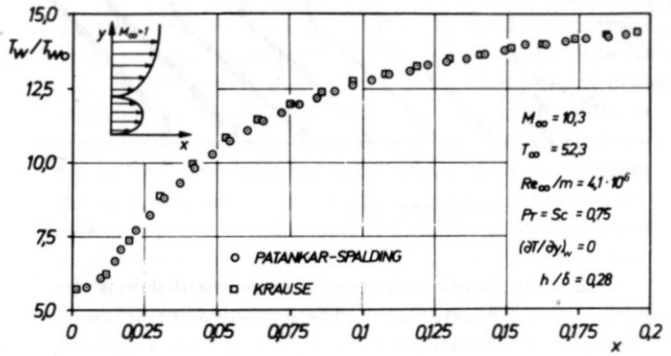

FIG. 17. Comparison of the Numerical Method of [7] and [8].

clearly evident and transition to turbulence could not be observed although the tangential injection of air causes a severe distortion of the velocity in the external boundary layer. The development of the static temperature distribution in the mixing region is shown in Fig. 16. Initially, constant temperature is observed near the slot, increasing to a maximum in the external boundary layer.

The numerical calculations reported in [6] were also tested with the numerical method of [8] and a comparison of wall temperatures as predicted by both methods for the case of an isolated wall demonstrates the reliability of the numerical results. The agreement with the experimental data indicated in Figs. 15 and 16 confirms the laminar nature of the flow in the mixing region. The small but noticeable deviation of the experimental results from the theoretical prediction is caused by a slow heating up of the model during the test, which usually lasted for about 20 minutes.

In Ref. [9] D.H. Chung extended this analysis and investigated the question of whether, for an isolated wall, the wall temperature depends stronger on the slot height than on the mass flux rate when the total injected mass is held constant. Helium, air and argon were assumed to be injected through the slot. The calculation was always halted at the point where the wall temperature starts to rise noticeably; that is to say when the local wall temperature exceeded its initial value in the slot by five percent. This criterion is arbitrary and the characteristic distance between the slot and the point of noticeable temperature rise depends on the temperature difference assumed to be characteristic for the problem. Fig. 18 shows this distance $(x/h)_k$ as a function of the dimensionless mass flux for $M_\infty = 10.24$ and $Re_\infty/m = 4 \cdot 10^6$. It is seen that the wall temperature exhibits a weaker dependence on the slot height than on the mass flux rate when the total mass injected through the slot is kept constant. This is particularly evident for helium, although this case is only of academic interest; the maximum Mach number in the slot would have to be much larger than those for air and argon injection in order to obtain the same mass flux entering through the slot.

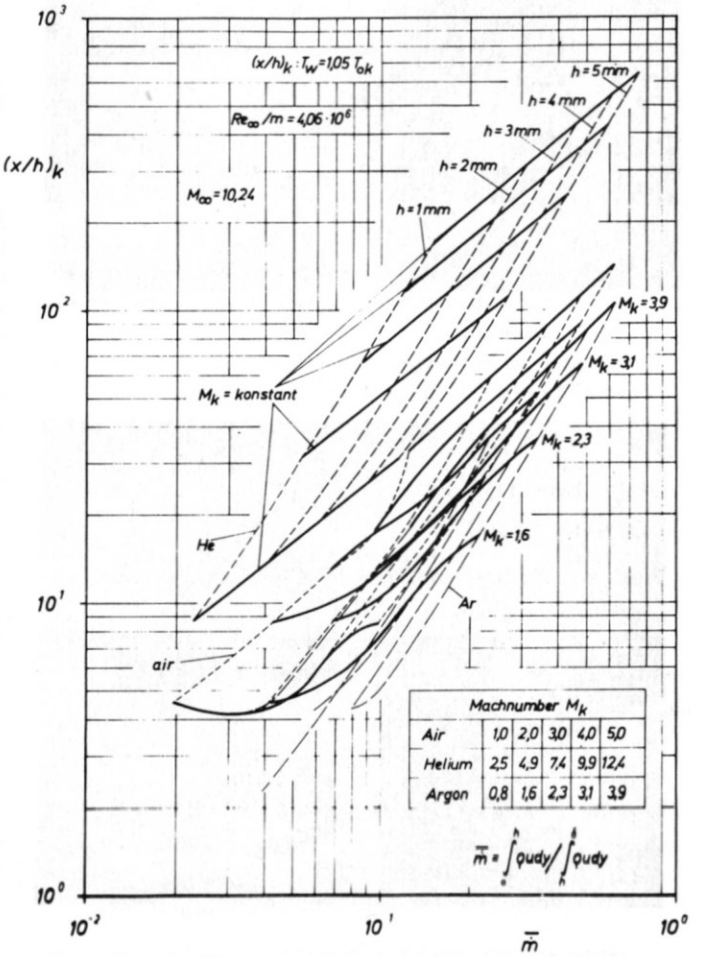

FIG. 18. Influence of Slot Height and Mass Flux Rate on the Wall Temperature.

First experimental results for helium injection are shown in Fig. 19 for a freestream Mach number of $M_\infty = 8.35$. Concentration profiles measured at various stations x/h are plotted versus the nondimensionalized coordinate y/h. The results are compared with predictions of the numerical solution described in the next section. It is seen that the predictions depend noticeably on the transport coefficients. In the outer part of the boundary layer the measurements agree quite well with the predictions of the numerical solution. The dashed lines are the mass concentration profiles for Pr- and Sc-numbers taken constant, and the

viscosity was evaluated for a two-component air-helium mixture. The initial data of the calculation were taken from the measurements at $x/h = 1.03$. The

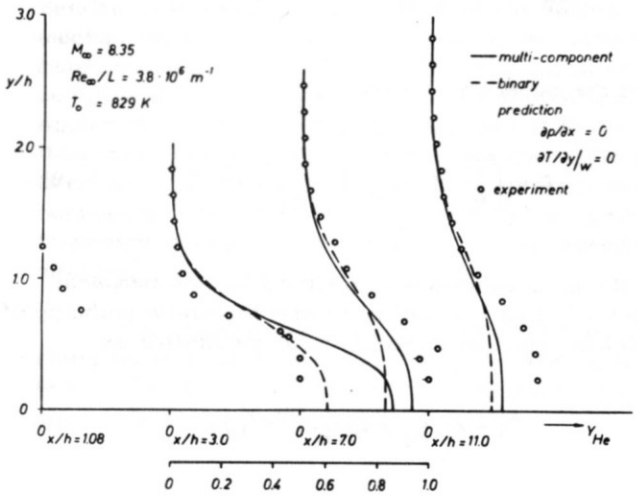

FIG. 19. Measured and Calculated Helium Profiles for Tangential Slot Injection.

solid lines show the profiles as calculated with all three diffusion fluxes (O_2, N_2, He) taken into account. Large deviations are noted in the vicinity of the slot where the concentration of the helium is large. The effect of pressure gradients has been neglected but is presently being investigated. A shift of the numerical predictions may be introduced when more exact expressions for the collision integrals are used in the equations for the viscosity the thermal conductivity and diffusion coefficient. For this calculation the rigid-sphere model was employed. The experimental data are most likely in error in the region close to the wall; further investigations will clarify the discrepancies of Fig. 19. As mentioned before, extremely long test durations are necessary to collect enough helium (in the probe) for an accurate measurement. Nevertheless the experimental data have been reproduced repeatedly.

The measurements are presently being extended to other Mach numbers. Further investigations will also include the influence of overpressure in the slot on the concentration decay, and it is planned to study such flows also theoretically.

Although there are large diffusion gradients on both sides of the plate the measurements along the center line do not seem to be affected for the results reported here. Later on, crosswise measurements of concentration profiles will be made in order to detect the influence of the finite width of the plate.

In the next section, the numerical solution used here for the calculation of the concentration profiles is briefly described.

Numerical Solution of the Boundary-Layer Equations for Tangential Slot Injection of a Foreign Gas at Limiting Reaction Rates

The Differential Equations

Heat release through hydrogen-oxygen reactions in laminar compressible boundary layers has been investigated by several authors. Because of the relative complex nature of the complete reaction system simple chemical models are often used to make an analysis possible. Examples of such models are given in [10], [11], [12], and [13]. In [10] a flame-zone model is employed according to which the flow in the neighbourhood of the temperature maximum is assumed to be in chemical equilibrium but chemically frozen when the temperature falls below a certain characteristic value. The limiting case of the flame-zone model is the flame-sheet approximation in which the thickness of the flame zone is reduced to zero [10]. Comparison calculations to exact equilibrium conditions show that the flame sheet approximation gives realistic results for temperatures below 3000 K but introduces a discontinuity in the concentration gradients at the temperature maximum. This is not a serious draw-back as the exact equilibrium profiles exhibit also a rapid change at the flame sheet. Its major advantage is that the cumbersome determination of the equilibrium constant for every step of integration is eliminated in the numerical solution.

The shape of the profiles of the flow variables is affected by the transport properties chosen for the investigation. The influence of the various chemical components on the diffusion fluxes is investigated in [11] and [12]. Therein it is shown that for a reactive hydrogen-air mixture the binary gas approximation deviates considerably from the multi-component representation. The investigations of Refs. [10], [11], and [12] were restricted to similar and one-dimensional flows, respectively. For that reason, it had to be assumed that the hydrogen is injected normal to the wall. Because of the similarity conditions in [10] and [11] only those flows could be investigated for which the normal velocity component at the wall is proportional to $x^{-1/2}$. By the use of numerical solutions as in the present investigation also nonsimilar flows as specified in a complete initial-boundary-value problem can be analysed. Consequently, arbitrary (within certain limitations) initial profiles may be prescribed. It is assumed here that the chemical model as well as the representation of the diffusion fluxes are the same as those of Ref. [11]. The boundary-layer equations to be used here then read:

Global continuity equation

$$\frac{\partial}{\partial x}(\rho u) + \frac{\partial}{\partial y}(\rho v) = 0 \qquad (1)$$

Momentum equations

$$\rho u \frac{\partial u}{\partial x} + \rho v \frac{\partial u}{\partial y} = -\frac{\partial p}{\partial x} + \frac{\partial}{\partial y}\left(\mu \frac{\partial u}{\partial y}\right)$$
$$\frac{\partial p}{\partial y} = 0 \qquad (2)$$

Energy equation

$$\rho u \frac{\partial H}{\partial x} + \rho v \frac{\partial H}{\partial y} = \frac{\partial}{\partial y}\left[\frac{\mu}{Pr}\frac{\partial H}{\partial y} - \sum_{i=1}^{N} h_i\left(J_i + \frac{\mu}{Pr}\frac{\partial Y_i}{\partial y}\right) + \right.$$
$$\left. + E_\infty\left(1 - \frac{1}{Pr}\right)\mu u \frac{\partial u}{\partial y}\right] \qquad (3)$$

Species continuity equations

$$\rho u \frac{\partial Y_i}{\partial x} + \rho v \frac{\partial Y_i}{\partial y} = -\frac{\partial J_i}{\partial y} + \dot{\omega}_i \qquad i = 1, \ldots N \qquad (4)$$

Elements continuity equations

$$\rho u \frac{\partial \tilde{Y}_j}{\partial x} + \rho v \frac{\partial \tilde{Y}_j}{\partial y} = -\frac{\partial}{\partial y}\left(\sum_{i=1}^{N} \mu_{ij} \frac{W_j}{W_i} J_i\right) \qquad (5)$$
$$j = 1, \ldots L$$

As standard notation is used (see for example Ref. [14]) for all variables no further explanations for the notation need be given; it suffices to mention that all symbols represent nondimensionalized variables with the normal velocities (including the diffusion velocity) and the coordinate normal to the wall being stretched by the square root of the Reynolds number. The above equations are supplemented by the definition of the mass fraction of the elements

$$\tilde{Y}_j = \sum_{i=1}^{N} \mu_{ij} \frac{W_j}{W_i} Y_i \qquad (6)$$

the sums

$$\sum_{i=1}^{N} Y_i = 1 \;, \quad \sum_{j=1}^{L} \tilde{Y}_j = 1 \;, \quad \sum_{i=1}^{N} \vec{J}_i = 0 \;, \qquad (7)$$

and the equation of state

$$\rho = \left(\sum_{i=1}^{N} Y_i / W_i\right)_e \Big/ \left(T \sum_{i=1}^{N} Y_i / W_i\right) \qquad (8)$$

A linear dependence is assumed for the temperature - enthalpy relation so that the static enthalpy of the i-th chemical component can be written as

$$h_i = \Delta_{i,T_{ref}} + c_{p_i T_{ref}} (T - T_{ref}) \qquad (9)$$

For the solution of the differential equations (1) - (5) initial - and boundary conditions must be prescribed. If the location of the slot is assigned the coordinate x = 0, then the initial conditions can formally be written in the following form:

$$\begin{cases} u(0,y) = f_1(y) \\ H(0,y) = f_2(y) \\ Y_i(0,y) = f_3(y) \;\; \text{or} \;\; \tilde{Y}_j(0,y) = f_4(y) \end{cases} \qquad (10)$$

The boundary conditions at the outer edge of the boundary layer are ($y \to \infty$):

$$\lim_{y\to\infty} \begin{Bmatrix} u(x,y) \\ H(x,y) \\ Y_i(x,y) \;\; \text{or} \;\; \tilde{Y}_j(x,y) \end{Bmatrix} = \begin{Bmatrix} u_e(x) \\ H_e(x) \\ Y_{ie}(x) \;\; \text{or} \;\; \tilde{Y}_{je}(x) \end{Bmatrix} \qquad (11)$$

At the wall (y = 0) the boundary conditions for an impermeable wall are

$$u \equiv 0 \;, \quad v \equiv 0 \;, \quad J_i(x,0) \equiv 0$$
$$H(x,0) = f_5(x) \;\; \text{or} \;\; \frac{\partial H}{\partial y}(x,0) = f_6(x) \qquad (12)$$

The above set of equations (1) - (12) must be made determinate by a mathematical description of the chemical model and the transport properties. This will be given in the next section.

Chemical Model and Transport Properties

The solution of the species continuity equations (4) requires the chemical source terms to be specified when the reaction rate is finite. As the detailed mathematical description of the reaction mechanism through the law of mass action complicates the integration of the differential equation considerably only the limiting cases of chemical equilibrium (infinite reaction rate) and of frozen flow (zero reaction rate) will be considered here. Such an idealization seems justified as the primary purpose of the investigation is to study the laminar transport mechanism of a reacting four-component mixture.

For completeness sake, some of the derivations given already in [11] and [13] are repeated here: For equilibrium conditions the four relevant reactions are according to [14]

$$\left\{\begin{array}{ll} 1. & \frac{1}{2}O_2 \rightleftharpoons O \\ 2. & \frac{1}{2}H_2 \rightleftharpoons H \\ 3. & \frac{1}{2}O_2 + \frac{1}{2}H_2 \rightleftharpoons OH \\ 4. & H_2 + \frac{1}{2}O_2 \rightleftharpoons H_2O \end{array}\right. \qquad (13)$$

Up to temperatures of the order of 3000 K the last reaction is the dominant one as its equilibrium constant is much larger than those of the other reactions: ($K_{p4} \cong 170\ K_{p1} \cong 130\ K_{p2} \cong 20\ K_{p3}$). If K_{p1}, K_{p2}, and K_{p3} are neglected, the mass fractions of the species Y_1 - Y_3 (the subscripts 1, 2, 3, and 4 denote O_2, H_2, H_2O, and N_2, respectively) are related to K_{p4} as follows:

$$K_{p4} = \left(\frac{Y_3}{W_3}\right)(\rho W)^{-1/2}\left(\frac{Y_1}{W_1}\right)^{-1/2}\left(\frac{Y_2}{W_2}\right)^{-1} \qquad (14)$$

As K_{p4} is large for temperatures below 3000 K, either Y_1 or Y_2 must be small if the other quantities are assumed to be of order one. The flame-sheet approximation as used in [11] is obtained by letting $Y_1 = 0$ in the inner portion of the boundary layer and $Y_2 = 0$ in the outer portion. The only combustion product H_2O is then produced along the flame sheet which represents the common border of the two adjacent regions. Its location is defined by the conditions $Y_1 = Y_2 = 0$. From equation (6) this condition may be expressed through the element mass fractions:

$$\tilde{Y}_1 = Y_1 + \frac{W_1}{2W_3}Y_3 \qquad (15)$$

and

$$\tilde{Y}_2 = Y_2 + \frac{W_2}{W_3}Y_3 \qquad (16)$$

which yield the flame sheet condition with $Y_1 = Y_2 = 0$:

$$\tilde{Y}_2 = 2\frac{W_2}{W_1}\tilde{Y}_1 \qquad (17)$$

In the two regions just described the diffusion fluxes are derived from the relation given in [15]

$$\frac{1}{\rho}\sum_{j=1}^{N}\frac{1}{W_j D_{ij}}\left(Y_j\vec{J}_i - Y_i\vec{J}_j\right) = \sum_{j=1}^{N}\frac{1}{W_j}\left(Y_i\nabla Y_j - Y_j\nabla Y_i\right) \qquad (18)$$

$$i = 1,\ldots,N \qquad j \neq i$$

The diffusion flux of the nitrogen is chosen to be eliminated through the last of equation (7) from equation (18) so that only the fluxes j_1 and j_3 in the outer region and j_2 and j_3 in the inner region have to be considered. From equation (18) there result relations of the form

$$\alpha_1 j_{1,2} + \alpha_2 j_3 = \alpha_3 \qquad (19)$$

The quantities $\alpha_1 - \alpha_3$ are given in [10] and [13] and will not be repeated here. Inspection of equation (18) shows that $\alpha_1 - \alpha_3$ are, in general, functions of the binary diffusion coefficients D_{ij}, the molecular weights W_i, and the mass fractions Y_i. Equation (19) can be solved for j_1, j_2 and j_3 and all diffusion fluxes can then be calculated from the initial conditions. In the solution of the element equations two ways have been tried so far: First equation (5) was rewritten in conservative form

$$\frac{\partial}{\partial x}\left(\rho u\tilde{Y}_i\right) + \frac{\partial}{\partial y}\left(\rho v\tilde{Y}_i + \sum_{i=1}^{N}\mu_{ij}\frac{W_i}{W_i}J_i\right) = 0 \qquad (20)$$

and then solved numerically. In the second approach the diffusional fluxes were expressed through the derivatives $\partial\tilde{Y}_1/\partial y$ and $\partial\tilde{Y}_2/\partial y$ yielding second order equations for equation (5).

The equations for the transport coefficients D_{ij}, μ_i and k_i were taken from [15]:

The diffusion coefficients are given by

$$D_{ij} = 1.8583 \cdot 10^{-3} T^{3/2} \left(\frac{1}{W_i} + \frac{1}{W_j}\right)^{1/2} p^{-1} \sigma_{ij}^{-2} \quad cm^2/sek \tag{21}$$

and the viscosity and the thermal conductivity are obtained from the following relations:

$$\mu_i = 2.6693 \cdot 10^{-5} (W_i T)^{1/2} \sigma_i^{-2} \quad g/sek\ cm \tag{22}$$

$$k_i = \left(c_{p_i} + \frac{5}{4}\frac{R}{W_i}\right)\mu_i \quad cal/cm\ sek\ K \tag{23}$$

The viscosity and the thermal conductivity of the mixture were calculated from the equations

$$\left.\begin{matrix}\mu \\ k\end{matrix}\right\} = \sum_{i=1}^{N} \left[\left(Y_i/W_i\right) \Big/ \left(\Phi_{ij} \sum_{j=1}^{N} Y_j/W_j\right)\right] \left\{\begin{matrix}\mu_i \\ k_i\end{matrix}\right\} \tag{24}$$

with

$$\Phi_{ij} = 8^{-1/2}\left(1 + \frac{W_i}{W_j}\right)^{-1/2}\left[1 + \left(\frac{\mu_i}{\mu_j}\right)^{1/2}\left(\frac{W_j}{W_i}\right)^{1/4}\right]^2 \tag{25}$$

These equations complete the auxiliary relations for the differential equations (1) - (5), which now can be solved numerically. The major steps of the development of the difference equations are outlined in the next section.

Finite Difference Equations

Numerical solutions for the equations (1) - (5) have been given by several authors. In finite difference solutions mainly three different types of finite difference approximations are employed: The implicit Crank-Nicholsen and Laasonen schemes, and the explicit scheme. The implicit schemes are, in general, preferred since they are unconditionally stable and do not impose limitations on the step size as is true for explicit integration. Of the three schemes the Crank-Nicholsen scheme has the smallest truncation error. If, however, source terms or lower order terms are so large that the step size Δx in the stream-wise direction has to be smaller than Δy the Laasonen scheme requires fewer computational steps than the Crank-Nicholsen scheme without loss in accuracy. If eventually the step size Δx must be smaller than $(\Delta y)^2$ implicit integration does not offer any further advantage. For this reason all three schemes were used in the numerical solution. The details as well as the discretization procedure were carried out by W. Kordulla and are described in [16]. The derivation of the difference equations follows very much the method of Ref. [8]. Some special considerations are, however, necessary in order to adapt the numerical solution for the problem being investigated here. One modification had to be made for the two-layer problem described earlier in the flame-sheet approximation. For each step of integration the location of the flame sheet must be determined before the integration of the flow variables can be initiated. This can be done by calculating the slope of the flame sheet from the initial data. In order to do so it is convenient to choose either Y_1 or Y_2 as they both vanish at the flame sheet, i.e.:

$$\frac{dY_1}{ds} = \frac{dY_2}{ds} = 0 \tag{26}$$

The coordinate s is measured along the flame sheet. The total derivatives in equation (26) are substituted by the partial derivatives with respect to x and y, and the slope dy/dx. The x-derivatives are eliminated through the species continuity equation with i set either 1 or 2. There results then

$$\frac{dY}{dx} = \frac{v}{u} + \left[\frac{\partial J_1}{\partial y} \Big/ \left(\rho u \frac{\partial Y_1}{\partial y}\right)\right]^{+} = \frac{v}{u} + \left[\frac{\partial J_2}{\partial y} \Big/ \left(\rho u \frac{\partial Y_2}{\partial y}\right)\right]^{-} \tag{27}$$

The superscripts (+) and (-) indicate that the derivatives of the diffusion fluxes and the mass fractions have to be evaluated from the initial data in the outer region (+) or from the inner region (-), respectively, at the location of the flame sheet.

Equation (27) presupposes that the jump condition for the fluxes as derived by Libby and Pierucci in [11] for similar flows is also valid for non-similar flows. This can be shown to be true by the use of an integral of one of the elements equations (5) with, e.g., j = 2. If equation (20), which is equivalent to equation (5) is integrated with respect to y there is obtained

$$\frac{d}{dx}\int_0^{\infty} \rho u \tilde{Y}_2\, dy + \rho v \tilde{Y}_2 \Big|_0^{\infty} - \sum_{i=1}^{N} \left(\mu_{i2} \frac{W_2}{W_i} J_i\right)\Big|_{-}^{+} = 0 \tag{28}$$

where the plus and minus sign indicate again outer and inner region, respectively, at the location of the flame sheet. Since v vanishes for y = 0 and $\tilde{Y}_2$ for $y \to \infty$, the second term in equation (28) is zero.

The integral represents the total mass flux of the element H. As this quantity must remain constant its derivative vanishes so that only the term involving the diffusion fluxes remains, yielding the jump condition of Ref. [11]. Arguments similar to those given above hold true for all other flow quantities so that all conditions derived in [11] for similar flows are also valid for non-similar flows. Since the first derivatives of the mass fractions are discontinuous across the flame sheet, the differential equations (1) – (5) are not valid there. They must be replaced by the flame sheet conditions in order to enable the double integration in the direction normal to the wall over both regions. The transition from the inner to the outer region will be shown for the case of $\tilde{Y}_2$. All other quantities can be computed in a manner similar to the one outlined below.

The implicit difference form of equation (5) or its equivalent, equation (20), may be written as follows:

$$m_{1j}\,\tilde{Y}_{2(j+1)} + m_{2j}\,\tilde{Y}_{2(j)} + m_{3j}\,\tilde{Y}_{2(j-1)} + m_{4j} = 0 \qquad (29)$$

The coefficients $m_{1(j)} - m_{3(j)}$ and $m_{4(j)}$ depend on the coefficients of the differential equation and on the difference scheme employed in the discretization. To arrive at equation (29) one must assume that the diffusion flux resulting from H_2 and H_2O or O_2 and H_2O that of N_2 being eliminated by equation (7) is contained in the term m_{4j}. This form implies that equation (29) has been decoupled from the difference equation for $\tilde{Y}_1$. It is also possible to obtain coupled difference equations for all elements. The form chosen here is, however, better apted to demonstrate the application of the flame-sheet condition. If variable step sizes are used in the integration, m_{1j}–m_{4j} are adjusted such that the location of the flame sheet is designated by the subscript j + 1, and the mesh points in the y-direction just below the flame sheet by j and j – 1. In equation (29) the mass fraction $\tilde{Y}_{2(j-1)}$ can be eliminated with the recursion relation [16]

$$\tilde{Y}_{2(j-1)} = A_{1(j-1)}\,\tilde{Y}_{2j} + A_{2(j-1)} \qquad (30)$$

and equation (29) is recasted into the form

$$\tilde{Y}_{2j} = A_{1j}\,\tilde{Y}_{2(j+1)} + A_{2j} \qquad (31)$$

If the mass fraction at the flame sheet $\tilde{Y}_{2(j+1)}$ is known $\tilde{Y}_{2(j)}$ can also be computed. The finite difference equation on the other side of the flame sheet is – under the same assumptions – as before

$$m_{1(j+2)}\,\tilde{Y}_{2(j+3)} + m_{2(j+2)}\,\tilde{Y}_{2(j+2)} + m_{3(j+2)}\,\tilde{Y}_{2(j+1)} + m_{4(j+2)} = 0 \qquad (32)$$

Equation (32) shows that the expressions in the recursion relations $A_{1(j+1)}$ and $A_{2(j+1)}$ cannot be obtained unless the jump conditions are introduced. The finite difference form of equation (28) is

$$n_{1(j+2)}\,\tilde{Y}_{2(j+3)} + n_{2(j+2)}\,\tilde{Y}_{2(j+2)} + n_{3(j+2)}\,\tilde{Y}_{2(j+1)} + n_{4(j+2)}\,\tilde{Y}_{2j} + n_{5(j+2)}\,\tilde{Y}_{2(j-1)} + n_{6(j+2)} = 0 \qquad (33)$$

With this relation $A_{1(j+1)}$ and $A_{2(j+1)}$ result from equations (30) – (33) by eliminating $\tilde{Y}_{2(j-1)}$, $\tilde{Y}_{2(j)}$ and $\tilde{Y}_{2(j+3)}$.

$$A_{1(j+1)} = \left[n_{1(j+2)}m_{2(j+2)} - n_{2(j+2)}m_{1(j+2)}\right]/D \qquad (34)$$

$$A_{2(j+1)} = \left\{n_{1(j+2)}m_{6(j+2)} - \left[\left(n_{5(j+2)}A_{2(j-1)} + n_{6(j+2)}\right) + A_{2j}\left(n_{4(j+2)} + n_{5(j+2)}A_{1(j-1)}\right)\right]m_{1(j+2)}\right\}/D \qquad (35)$$

$$D = \left[n_{3(j+2)} + A_{1j}\left(n_{4(j+2)} + n_{5(j+2)}A_{1(j-1)}\right)\right]m_{1(j+2)} - m_{3(j+2)}n_{1(j+2)} \qquad (36)$$

The recursion relations (34) – (36) enable the computation across the flame sheet and the formalism demonstrated here can be extended to all other flow variables.

Another point to be mentioned is the accuracy of the solution. It has already been noted by other authors that the numerical solution may become inaccurate or even unstable when one boundary condition is given by a vanishing derivative normal to the wall. In order to detect inaccuracies of this type the mass flux of the elementary hydrogen was determined for every step of integration in the streamwise direction. As pointed out earlier the integral $\int_0^\infty \rho u\,\tilde{Y}_2\,dy$ must remain constant and since its exact value is known errors in the calculation can easily be detected. It was found that for frozen flows no difficulties arise. However, large mass differences were noted in the multi-component-diffusion calculations of reactive hydrogen-air mixtures. Even when equation (7) is satisfied within an error of 10^{-8} the total elementary mass flux of the hydrogen did not remain constant. This could only be repaired when very small step sizes were used in the calculation. For this reason fourth

order finite difference approximations are being tested in order to reduce the truncation error which seems to act as source term on the boundaries [16].

Results of Sample Calculations

In this final section some results are reported which were obtained from the numerical solution briefly described in the last section. Fig. 20 shows the concentration profiles for an air-hydrogen mixture

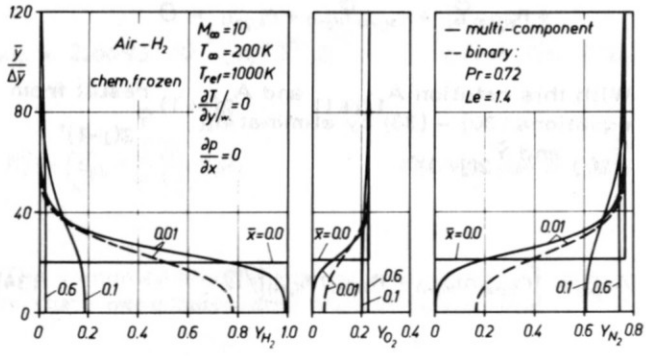

FIG. 20. Calculated Concentration Profiles. Frozen Flow

as injected through a tangential slot. The profiles are given at various x-stations ($\bar{x}$ being the physical coordinate referenced to the characteristic length of the Reynolds number). It is noted that the profiles for the binary gas approximation differ considerably from those with multi-diffusion effects included. This shows that constant Pr- and Le-numbers are not a realistic approximation for the mixture. The corresponding concentration profiles for the flame-sheet approximation are shown in Fig. 21. Here only profiles for the binary gas approximation are reported. The plot in the middle of Fig. 21 shows the profiles for H_2O. It can be seen how the reaction product increases in the streamwise direction. The location of the flame sheet is indicated by the discontinuous first derivatives. The results of the multi-component calculation for the reactive hydrogen-air mixture are presently being checked. They indicate (as for frozen flows) a behaviour different from those shown here. In Fig. 22 the mass fractions as obtained for y = 0 are plotted versus the non-dimensionalized coordinate x/h. Inspite of the fact that the mixing process is laminar a steep decay can be noted in all cases. As the amount of H_2O produced immediately downstream from the slot is small the curves for the reactive and the non-reactive system are almost identical. Only further downstream do they differ from each other. Figs. 23 and 24 give a comparison of the temperature profiles for a chemical frozen flow and a flow in chemical equilibrium. The

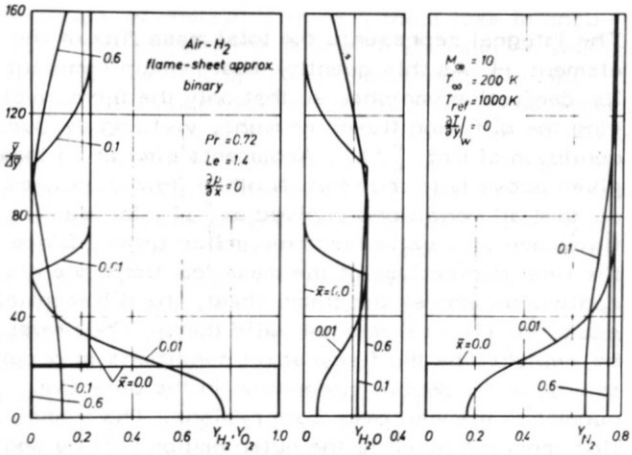

FIG. 21. Calculated Concentration Profiles. Flame-Sheet Approximation

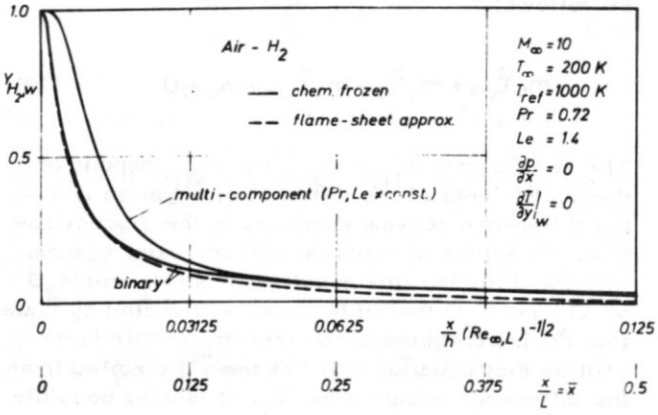

FIG. 22. Calculated Concentration at the Wall.

change of the temperature profiles due to heat release is clearly indicated. The corresponding curves of maximum temperatures are plotted in Fig. 25 versus x/h. As the temperature maxima were determined for the limiting cases of zero and infinite reaction rates, it can be concluded from this figure that the solution for the actual flow lies within the region bounded by these two curves. Fig. 26 finally shows a comparison of the shearing stress at the wall for the three cases discussed. All curves approach asymptotically the $1/\sqrt{\bar{x}}$-behaviour. The minimum immediately downstream from the slot is caused by the low-momentum flow of the hydrogen.

Some results have also been obtained for turbulent non-reactive flows at $M_\infty = 4$. In these calculations Michel's model for the mixing length [17] was used in the solution of the momentum equation and turbulent Pr- and Le-numbers were specified as

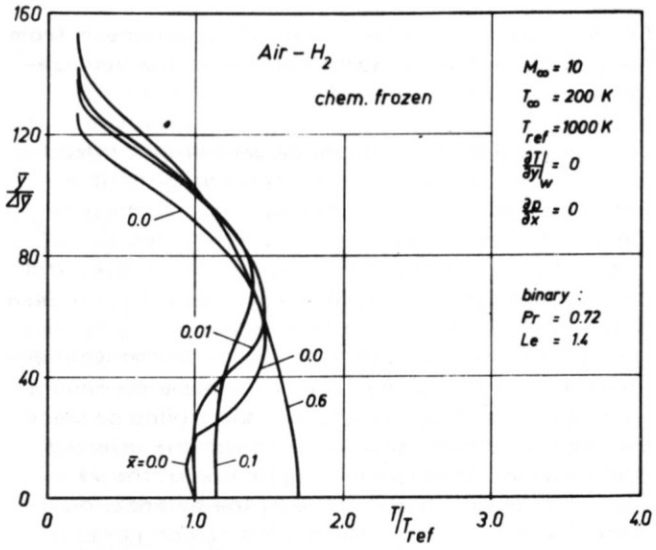

FIG. 23. Calculated Temperature Profiles. Frozen Flow

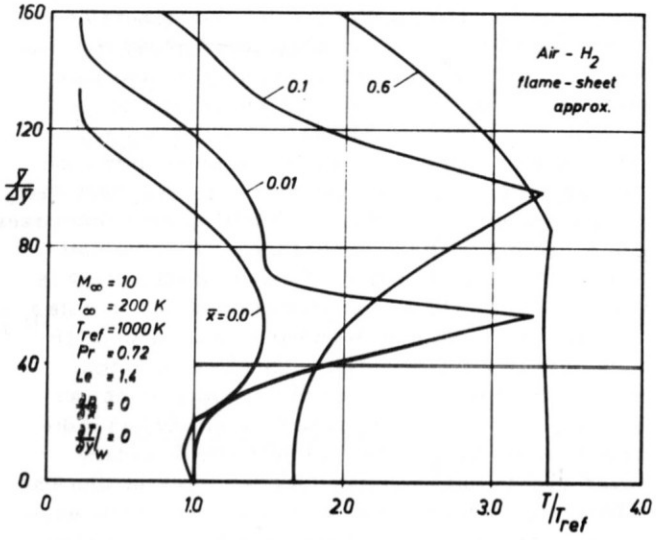

FIG. 24. Calculated Temperature Profiles. Flame-Sheet Approximation

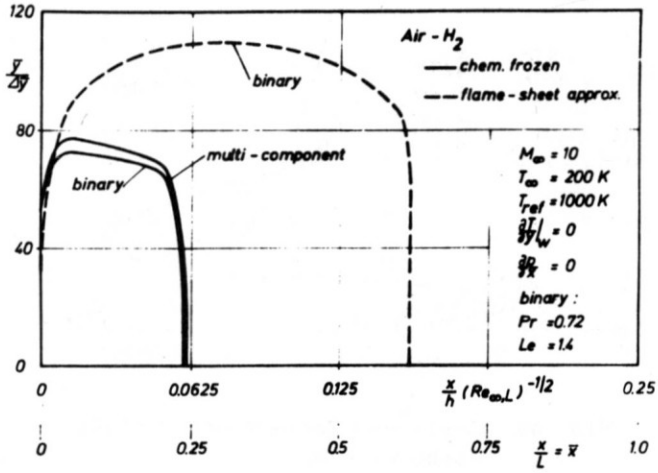

FIG. 25. Location of Maximum Temperatures. Frozen Flow and Flame-Sheet Approximation

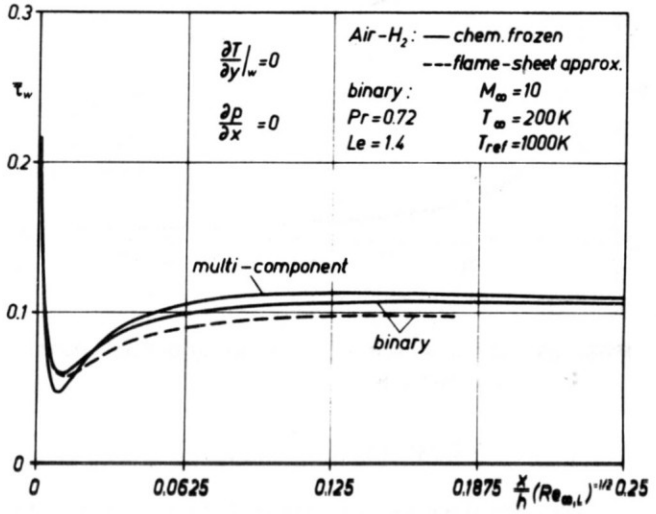

FIG. 26. Shearing Stress at the Wall.

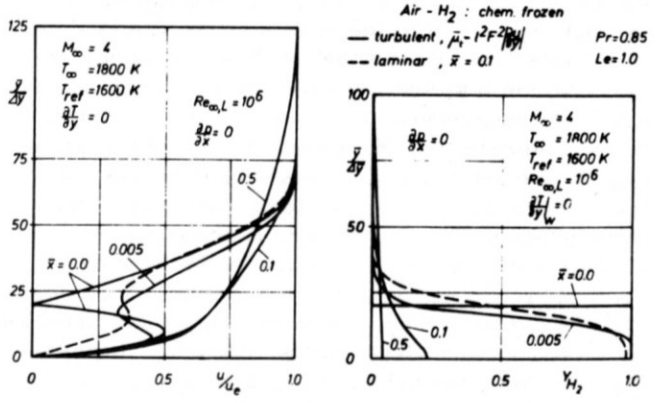

FIG. 27. Calculated Velocity and Concentration Profiles. Turbulent Flows

indicated in Fig. 27 and 28 where velocity-, concentration-profiles of hydrogen and temperature profiles are shown. For the sake of comparison the profiles for laminar flows at $\bar{x} = 0.1$ are also included. The concentration decay in particular shows the immediate mixing of the hydrogen with the air of the turbulent boundary layer. This is also visible in Fig. 29 where concentrations at $y = 0$ are plotted versus x/h for laminar and turbulent flow.

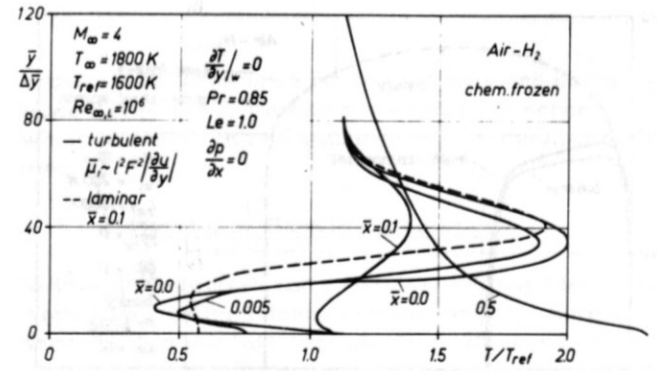

FIG. 28. Calculated Temperature Profiles. Turbulent Flows

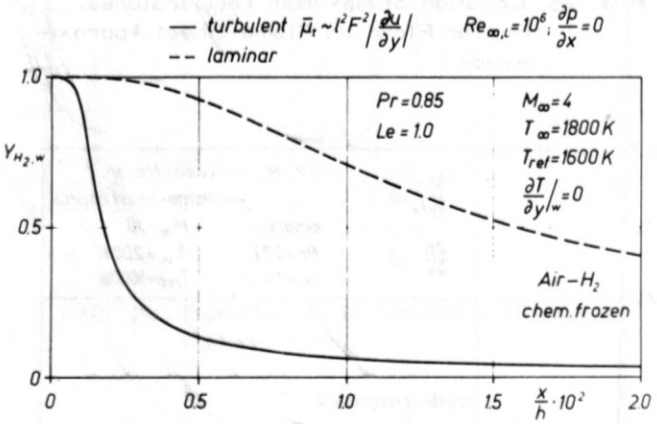

FIG. 29. Comparison of Laminar and Turbulent Concentration Decay.

Concluding Remarks

Results have been presented for two problems relating to supersonic and hypersonic combustion. In the first problem, which is studied experimentally, hydrogen is injected normal to the wall into the recirculation region generated upstream of a secondary stream of air also injected normally through the wall into the main stream. Combustion is initiated through a spark plug which is retracted from the test section when the flame has stabilized. Measurements of the wall pressure distribution indicate that the extent of the recirculation region is considerably increased due to heat release in the combustion process. The static pressure remains almost constant, decreasing only slightly from its maximum value in the vicinity of the slot for the secondary air injection. A decrease of the mass flux of the secondary air or an increase of the freestream Mach number causes a decrease of the maximum pressure and of the length of the recirculation region. As is shown here, the combination of injecting air and hydrogen normal to the wall can effectively be used to generate large side forces through aerodynamic spoiler action. The secondary stream of air also serves a second useful purpose as it protects the wall downstream from the slot from the high temperatures of the recirculation region.

In the second problem tangential slot injection is studied experimentally and theoretically at hypersonic Mach numbers. The primary purpose of the experiments is to study the mixing process of injected gas, combustible or non-combustible, with the by-passing air. Experimental results have been obtained for air and first preliminary results also for helium. Measurements of static- and stagnation-pressure, total temperature and volume concentration enable a clear insight into the mixing process downstream from the slot. Although the injected gas causes a considerable distortion of the velocity and temperature profile of the external boundary layer the flow in the mixing region remains laminar for all Reynolds numbers and Mach numbers investigated. The experimental data for air can accurately be predicted by numerical solutions of the boundary layer equations. For helium, the agreement between the experimentally and numerically determined concentration profiles is good in the outer portion of the boundary layer. Close to the wall, the accuracy of the measured data seems to be impaired by the low stagnation pressure. Numerical studies show that constant Pr- and Le-numbers do not adequately represent the actual transport mechanism. Close to the slot considerable deviations due to multi-component diffusion can be noted. Further numerical studies show that for an isolated wall, the wall temperature increases more rapidly with the mass flux rate in the slot than with the slot height, if the total mass flux is held constant. Rapid concentration decay is noted for laminar flows and even more pronounced for turbulent flows (computed with a mixing length model). Numerical studies of hydrogen injection and oxydation through chemical equilibrium indicate a steep temperature rise in the boundary layer due to heat release, suggesting that thermal diffusion, perhaps, should be included in the analysis. The chemical mechanism was simulated by the flame sheet model yielding H_2O as the only reaction product. By comparing the results of the flame sheet calculation with those obtained for frozen flow the extent of the flame can be estimated. The studies will be continued to investigate turbulent flows and flows with pressure gradients.

References

[1] Winterfeld, G., Report on Euromech 19: "Hypersonic Propulsion with Emphasis on Heat Addition to Supersonic Flows." Cologne, Germany, 15-17 December, 1970.

[2] Maurer, F., Wärmezufuhr im Überschall durch Verbrennung von Wasserstoff an einer tangential angeströmten Platte. 4. Jahrestagung der DGLR Baden-Baden, 11.-13. Oktober 1971. Vortrags-Nr. 71-094.

[3] Maurer, F., Wärmezufuhr im Überschall der Verbrennung von Wasserstoff an einer tangential angeströmten Platte. DFVLR-Institut für Angewandte Gasdynamik. DLR-FB 72-12, 1972.

[4] Pfeiffer, H., Will, E., Distelrath, H.-D., Der Hyperschallpilotkanal H 1 der DVL. Deutsche Versuchsanstalt für Luft- und Raumfahrt. DLR FB 69-44. Juli 1969.

[5] Pfeiffer, H., Will, E., Chung, D.H., Oberflächenkühlung in laminaren Hyperschallgrenzschichten. Vortrag auf dem XXI. Internationalen Astronautischen Kongreß, Konstanz (4.-10. Okt. 1970), DFVLR-Institut für Angewandte Gasdynamik, Porz-Wahn.

[6] Chung, D.H., Untersuchung der Wirkung einer Schleierkühlung in hypersonischen Grenzschichten an einer ebenen Platte. Diplomarbeit TH Aachen (Dez. 1969).

[7] Patankar, S.V., Spalding, D.B., A Finite-Difference Procedure for Solving the Equations of the Two-Dimensional Boundary-Layer, International Journal of Heat Mass Transfer, 10 (1967), pp 1389-1411.

[8] Krause, E., The Numerical Solution of the Boundary Layer Equation. AIAA Journal 5 (1966), S. 1231-1237.

[9] Chung, D.H., Theoretische Untersuchung der Wandkühlung in laminaren hypersonischen Grenzschichten, DLR Mitt. 71-13 (1971), S. 28-50.

[10] Libby, P.A., Economos, C., A Flame Zone Model for Chemical Reaction in a Laminar Boundary Layer with Application to the Injection of Hydrogen-Oxygen Mixtures. Int. J. Heat Mass Transfer 6 (1963), pp. 113-128.

[11] Libby, P.A., Pierucci, M., Laminar Boundary Layer with Hydrogen Injection Inciuding Multicomponent Diffusion, AIAA Journal, 2 (1964), pp 2118-2126.

[12] Graves, R.A., Diffusion Model Study in Chemically Reacting Air Couette Flow with Hydrogen Injection. NASA TR R-349, Oct. 1970.

[13] Kordulla, W., Krause, E., Energiezufuhr in laminaren Hyperschallgrenzschichten durch Wasserstoffverbrennung, DLR Mitt. 71-13 (1971), S. 76-101.

[14] Penner, S.S., Chemistry Problems in Jet Propulsion, The Macmillan Company, New York (1957).

[15] Bird, R.B., Stewart, W.E., Lightfoot, E.N., Transport Phenomena. John Wiley + Sons, 7th printing, 1966.

[16] Krause, E., Numerical Treatment of Boundary-Layer and Navier-Stokes Equations. Presented as part of the VKI Lecture Series "Numerical Methods in Fluid Dynamics" at the Von Kármán Institute for Fluid Dynamics. Rhode-Saint-Genèse, Belgium, 7-11 February 1972. DFVLR Techn. Memor. WT 1/72.

[17] Michel, R., Quémard, C., Eléna, M.-P., Turbulent Boundary Layer Velocity Distributions in a Uniform or Accelerated Compressible Flow, ONERA, T.P. No. 693 (1969).